Lead-Free Perovskite (Fe$_{1/2}$Ag$_{1/2}$)TiO$_3$ Nanoceramic: Synthesis and Characterization

Anal K. Jha[1,2], Sandeep Kumar[2], Naveen Kumar[1], Nitendra Kumar[1] and Prasad K[1,3*]

[1]*Aryabhatta Centre for Nanoscience and Nanotechnology, Aryabhatta Knowledge University, Patna 800001, India*
[2]*University Department of Chemistry, Tilka Manjhi Bhagalpur University, Bhagalpur 812007, India*
[3]*University Department of Physics, Tilka Manjhi Bhagalpur University, Bhagalpur 812007, India*

*Address for Correspondence
Prasad K, Aryabhatta Centre for Nanoscience and Nanotechnology, Aryabhatta Knowledge University, Patna 800001, India, E-mail: k.prasad65@gmail.com

Keywords: Nanoceramic; (Fe$_{1/2}$Ag$_{1/2}$)TiO$_3$; Citric acid gel method; Green synthesis; Dielectric constant; Magnetic properties

Abstract

Nanoceramic powder of (Fe$_{1/2}$Ag$_{1/2}$)TiO$_3$ having the particle sizes of 16-47 nm was synthesized using a citrate gel method. Energy dispersive X-ray, transmission electron microscope, X-ray diffraction and infrared spectroscopy were used to ascertain the formation of (Fe$_{1/2}$Ag$_{1/2}$)TiO$_3$ nanoceramic (FAT-nc). Heat of combustion, heat of dissociation of tartaric acid and combustion of organic present in the gel along with the evolution of gases during calcination created ambiance for reaction to occur more easily to form FAT-nc. UV-vis study exhibited the surface plasmon resonance at 322 nm. The ac conductivity is found to obey the universal power law. The FAT-nc powder was further pressed into disk and sintered at 800 °C for 3 h in air, and its microstructure, dielectric, impedance and magnetic properties were studies. Complex impedance analyses suggested the dielectric relaxation to be of non-Debye type. The pair approximation type correlated barrier hopping model is found to successfully explain the mechanism of charge transport in FAT-nc. Dielectric study revealed a low value of room temperature dielectric constant (= 171) and dielectric loss (= 0.49) at 1 kHz. Magnetic studies have been carried out using vibration sample magnetometer, which indicated the possibility of magnetoelectric coupling.

Introduction

Perovskite ABO$_3$-type structured materials have attracted widespread technological interest over the past few decades [1,2]. Among them, lead-bearing compounds such as - PbTiO$_3$, Pb(Zr,Ti)O$_3$, Pb(Mg$_{1/3}$Nb$_{2/3}$)O$_3$, etc. are widely used in microelectronic devices. However, it is known that lead has detrimental impact on environment which motivated a large group of researcher in order to replace PZT-based materials with lead-free materials for intended applications and one such promising material is Bismuth sodium titanate (Bi$_{1/2}$Na$_{1/2}$)TiO$_3$ (abbreviated as BNT). Recent works on the identical compound (Bi$_{0.5}$Ag$_{0.5}$)TiO$_3$ also showed excellent electrical properties [3,4]. During the past few years, several investigations have been made to study the electrical properties of (Bi$_{0.5}$Ag$_{0.5}$)TiO$_3$ - based solid solutions for their possible applications in microelectronic devices [5-8]. Further, bismuth is also considered as toxic and cause environmental pollution. Besides, it is known that synthesis process has a great influence on different properties of the materials. Therefore, the synthesis of pure and homogeneous material is a subject of great importance. It has been observed that ceramic materials synthesized using different soft-chemical methods exhibited improved properties compared to the same prepared by traditional solid state reaction method [3,4,9-13]. One such lead-free ceramic in this series is perovskite (Fe$_{1/2}$Ag$_{1/2}$)TiO$_3$ which is mechanically tough and ensure environment-friendly applications. Also, it is expected that this compound may show magneto-electric effect due to the iron-content. Furthermore, a low values of different magnetic parameters were displayed by (Ag$_{0.5}$Fe$_{0.5}$)TiO$_3$ nanoceramic prepared using stearic acid gel method with aqueous AgNO$_3$ [12].

Accordingly, with an aim of getting enhanced magnetic properties compared to the earlier one [12], present work reports the synthesis of a truly green (non-lead as well as bismuth free) (Fe$_{1/2}$Ag$_{1/2}$)TiO$_3$ nanoceramic (abbreviated as FAT-nc) using citric acid gel method and its structural (X-ray diffraction and its Rietveld analysis), microstructural (scanning (SEM) and transmission (TEM) electron microscopy), UV-Vis Spectroscopy, Fourier transformed infrared spectroscopy, electrical (dielectric, impedance and ac conductivity) and magnetic studies. For better understanding the system the dielectric relaxation study has been carried out. Besides, the correlated barrier hopping model has been applied to the ac conductivity data to ascertain the conduction mechanism of charge transport in FAT-nc. Also, an effort has been made to explain the mechanism for the synthesis of FAT-nc by citric acid gel method using simple principles of organic chemistry.

Experimental Details

Synthesis of (Fe$_{1/2}$Ag$_{1/2}$)TiO$_3$ nanoceramic

Figure 1 illustrates the flow diagram for the synthesis of fine powder of (Fe$_{1/2}$Ag$_{1/2}$)TiO$_3$ nanoceramic using citrate method. Reagent grade (purity > 99%) CH$_3$COOAg, Fe(NO$_3$)$_3$.9H$_2$O and citric acid from Aldrich and Titanium (IV) n-Butoxide (Ti(OC$_4$H$_9$)$_4$) from Acros were used as starting materials. First of all CH$_3$COOAg, Fe(NO$_3$)$_3$.9H$_2$O and Titanium (IV) n-Butoxide were weighed in proper stoichiometry. A known amount of citric acid was dissolved into deionized water in a beaker and the pH of the solution was adjusted to 7-8 by dropping an appropriate amount of ammonia solution (25%). After stirring at 70 °C for 1 h, titanium (IV) n-butoxide
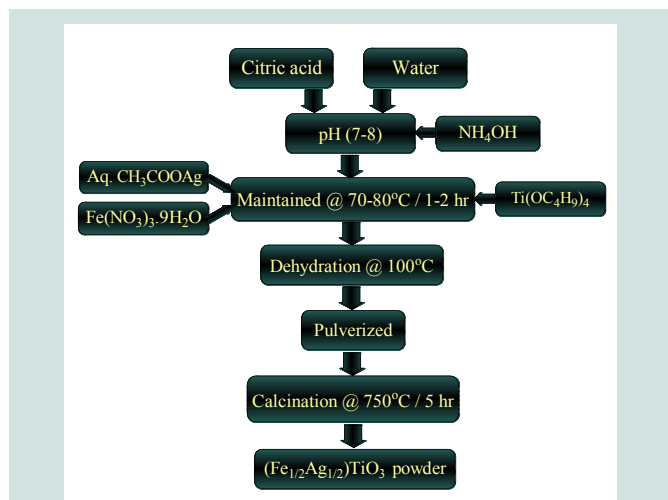
Figure 1: Flow chart showing preparation of $(Fe_{1/2}Ag_{1/2})TiO_3$ nanoceramic powder using citric acid gel method.
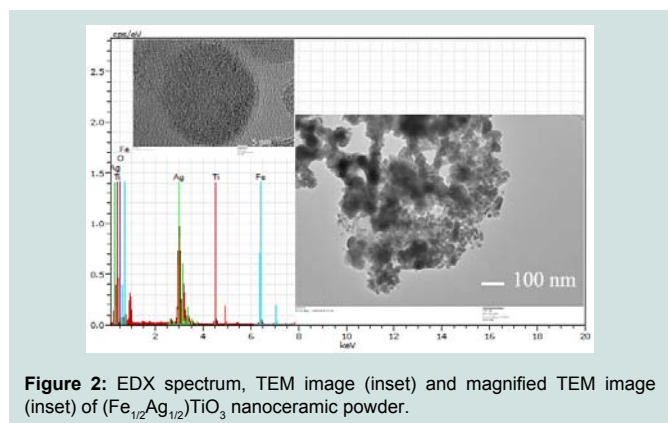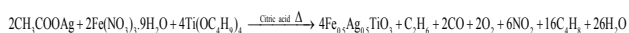

Figure 2: EDX spectrum, TEM image (inset) and magnified TEM image (inset) of $(Fe_{1/2}Ag_{1/2})TiO_3$ nanoceramic powder.

(XRD) analysis with CuK_α (= 1.5418Å) radiation (XPERT-PRO-PW3050/60, Pan Analytical). The XRD data were collected over the range of $2\theta = 20° - 80°$ with a step size of 0.02° with a count time of 2 s. TEM micrograph and energy dispersive X-ray (EDX) pattern of FAT-nc were obtained using High resolution Bruker transmission electron microscope, Germany. The surface morphology study was carried out using a scanning electron microscope (EVO 18, Carl Zeiss Microscopy Ltd., UK). The Fourier Transformed Infrared (FT-IR) spectrum of FAT-nc was collected in the transmission mode using an Alpha-T Bruker FTIR spectrophotometer in the range of 400-4000 cm^{-1}. The absorption spectrum of ultrasonically dispersed FAT-nc in absolute ethanol was obtained by a computer assisted UV-visible-NIR spectrophotometer (LAMBDA 950, PerkinElmer, UK). FT-IR spectra were measured by the transmission mode using an Alpha-T Bruker FTIR spectrophotometer with a wave number range of 4000 to 400 cm^{-1}. A sintered pellet was polished and electroded with air-drying silver paste (SPI supplier, USA) to measure the electrical properties. Dielectric and impedance measurements were carried out using a computer-interfaced impedance analyzer (E4990A-120, Keysight Technologies, USA). Magnetization behavior was studied using a vibrating sample magnetometer (model: 7410) Lake Shore Cryotronics, Inc., USA.
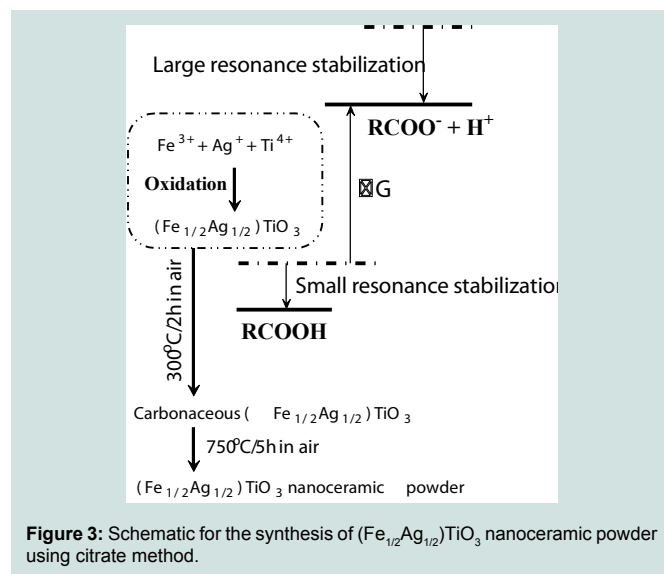

Figure 3: Schematic for the synthesis of $(Fe_{1/2}Ag_{1/2})TiO_3$ nanoceramic powder using citrate method.

was added into the solution and was further agitated for 1 h at 70 °C. This solution was further added with pre-prepared (40%) solution of CH_3COOAg in water and agitated for 1 h at same temperature. Now, pre-prepared (50%) solution of $Fe(NO_3)_3.9H_2O$ in water was added in above solution and was stirred at 80 °C for 2 h. The precursor solution was dehydrated at 110 °C to form a sol and subsequent heating at 160 °C yielded a gel. The gel initially started to swell and filled the beaker producing a foamy precursor. The gel was then pulverized and heated at 300 °C for 2 h in air atmosphere to get carbonaceous mass. The chemical reaction that takes place to form $(Fe_{1/2}Ag_{1/2})TiO_3$ nanoceramic powder is:

$$2CH_3COOAg + 2Fe(NO_3)_3.9H_2O + 4Ti(OC_4H_9)_4 \xrightarrow{Citric\ acid\ \Delta} 4Fe_{0.5}Ag_{0.5}TiO_3 + C_2H_6 + 2CO + 2O_2 + 6NO_2 + 16C_4H_8 + 26H_2O$$

Finally, the carbonaceous mass was calcined at 750 °C for 5 h. Completion of the reaction and formation of the desired compound was checked by X-ray diffraction technique. The as-calcined powder was compacted into thin (~1.5 mm) cylindrical disks with an applied uniaxial pressure of 650 MPa. The pellets were then sintered at 800 °C for 3 h in air atmosphere.

Characterization

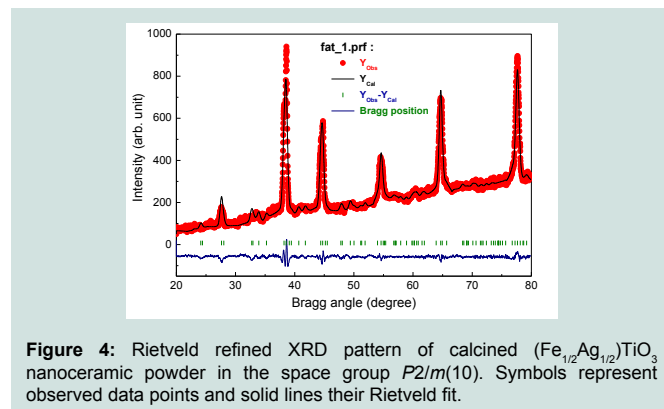The crystal structure was obtained by powder X-ray diffraction

Figure 4: Rietveld refined XRD pattern of calcined $(Fe_{1/2}Ag_{1/2})TiO_3$ nanoceramic powder in the space group $P2/m(10)$. Symbols represent observed data points and solid lines their Rietveld fit.
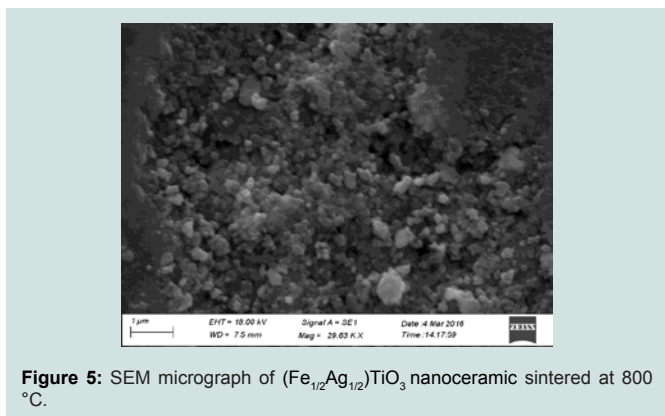
Figure 5: SEM micrograph of $(Fe_{1/2}Ag_{1/2})TiO_3$ nanoceramic sintered at 800 °C.
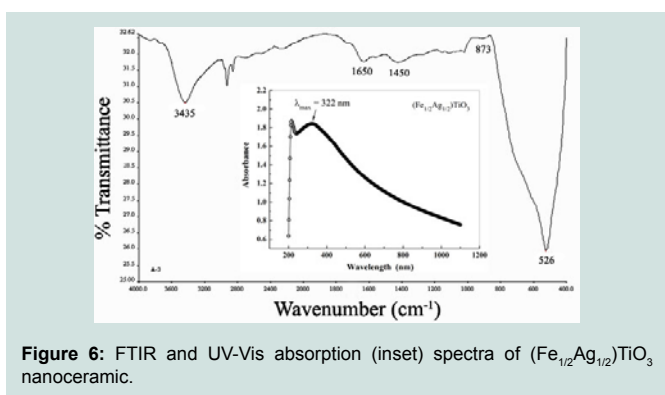

Figure 6: FTIR and UV-Vis absorption (inset) spectra of $(Fe_{1/2}Ag_{1/2})TiO_3$ nanoceramic.

Results and Discussion

Figure 2 shows the EDX pattern and TEM image (inset) of FAT-nc. All the peaks in the EDX pattern have perfectly been assigned to the elements present in $(Fe_{1/2}Ag_{1/2})TiO_3$, which clearly indicated the successful synthesis and purity of chemical composition of FAT-nc. The TEM image shows the distribution of particle sizes ranging between 16 to 47 nm. Apart from spherical particles, few elongated and bigger particles could be seen in the TEM image, this might be due to the agglomeration of nanoparticles or adherence of one nanoparticle to the other. A magnified TEM image (inset) clearly shows the formation of spherical nanoparticle of ~40 nm size.

Figure 3 depicts the schematics for the synthesis of FAT-nc using citric-acid gel method. It is observed that citric acid and citrate ions are readily inter-convertible in aqueous medium requiring and/or releasing an appreciable amount of free energy ($\Delta G \sim 47$ KJ/mol) [11,14,15] which is probably sufficient enough for nano-transformation. The nucleation and growth theory to form a spherical particle could be applied to understand mechanism of present nano-transformation and according to which the overall free energy change must be overcome. Also, $\Delta G = -\frac{4}{V}\pi r^3 k_B T \ln(S) + 4\pi r^2 \gamma$, where V, r, k_B, S and γ are the molecular volume of the prepared species, radius of the nucleus, Boltzmann constant, saturation ratio and surface free energy per unit surface area, respectively gives indication about the sum of free energy due to the formation of a new volume and the new surface created. It follows from equation that a decrease in γ or an increase in S is helpful in the formation of nanoceramic (FAT-nc, in this case). Besides, R-COOH makes a non-equivalent resonating structure

whereas RCOO$^-$ efficiently makes an equivalent one. This way, the resonance energy of stabilization of R-COOH is larger than that of RCOO$^-$ and this energy of dissociation probably remains available all along in the incubation medium for nano-transformations [14,15]. In the present synthetic method, the interactions of citric acid with Fe^{3+}, Ag^+ and Ti^{4+} ions in proper stoichiometric ratio made it possible to lower down the surface energy. Upon heating the mixture, the solvent (water) evaporates resulting in increased viscosity. After complete removal of water, the mixture turns into a gel form and its constituents are mixed at atomic level. This gel upon further heating at higher temperature (750 °C/5 h) produces $(Fe_{1/2}Ag_{1/2})TiO_3$ nanoceramic powders, which might be due to the combustion of organics present in the gel, along with the evolution of gases during calcination. Therefore, the effect of such soft-chemical ambiance could have made the reaction to occur more easily.

The structural refinement of FAT-nc was carried out using FullProf software employing the Rietveld refinement method. The broadening of XRD peaks indicated the formation of nanoscale particles. Also, it can be seen that pure perovskite type nanocrystalline FAT was formed at 750 °C and no other intermediate phase is observed. The Rietveld refined results showed good agreement ($\chi^2 = 0.561$) between the measured experimental XRD pattern and theoretical line profile (Figure 4). Besides, a very small difference between experimentally observed (Y_{Obs}) and theoretically calculated (Y_{Calc}) XRD data could be seen. The XRD analyses indicated that FAT-nc has a monoclinic structure having the space group $P2/m(10)$. The lattice parameters $a = 5.2851Å$, $b = 4.0804Å$, $c = 5.090Å$ and $\beta = 90.657°$. Further, a linear least square fitting of $B\cos\theta$-$\sin\theta$ data to Williamson-Hall equation: $B\cos\theta = (K\lambda/D) + 2(\Delta\xi/\xi)\sin\theta$, where B is diffraction peak width at half intensity and $\Delta\xi/\xi$ is the lattice strain, K is the Scherrer constant (0.89) and the term $K\lambda/D$ represents the Scherrer
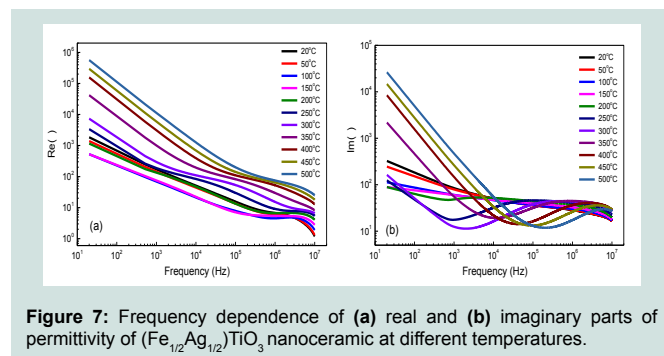

Figure 7: Frequency dependence of **(a)** real and **(b)** imaginary parts of permittivity of $(Fe_{1/2}Ag_{1/2})TiO_3$ nanoceramic at different temperatures.
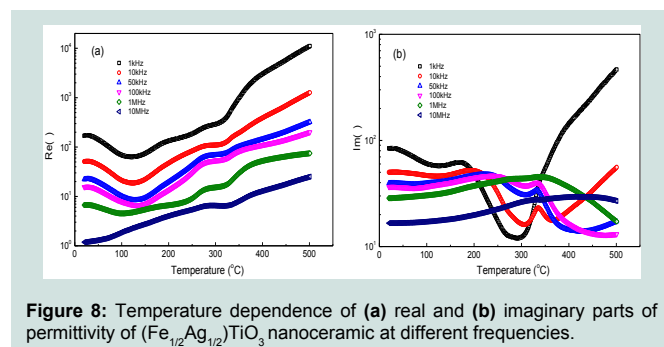

Figure 8: Temperature dependence of **(a)** real and **(b)** imaginary parts of permittivity of $(Fe_{1/2}Ag_{1/2})TiO_3$ nanoceramic at different frequencies.
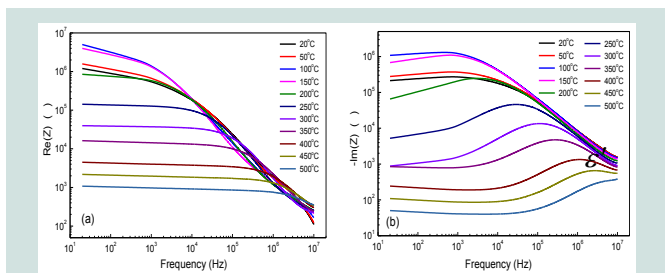
Figure 9: Frequency dependence of **(a)** real and **(b)** imaginary parts of impedance of $(Fe_{1/2}Ag_{1/2})TiO_3$ nanoceramic at different temperatures.
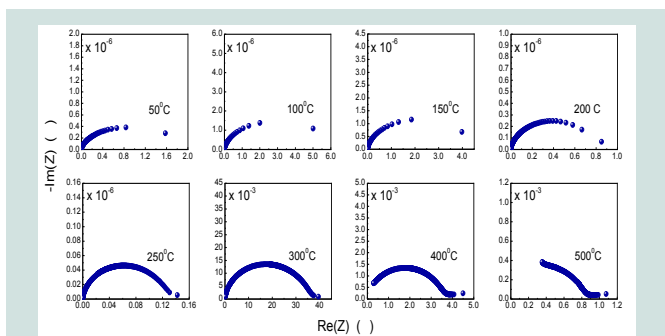

Figure 10: Complex impedance plots of $(Fe_{1/2}Ag_{1/2})TiO_3$ nanoceramic at different temperatures.

particle size distribution, yielded the value of apparent particle size to be 34 nm.

Figure 5 shows the SEM micrograph of sintered FAT-nc sample. The grains having spherical shapes of unequal sizes (~100-200 nm) appear to be distributed throughout the sample. Besides, a very few soft agglomerations of grains could be seen in the SEM micrograph.

The FT-IR spectrum of $(Fe_{1/2}Ag_{1/2})TiO_3$ nanoceramic powder is depicted in Figure 6. The spectrum exhibits a prominent fundamental absorption peaks at 526 cm^{-1} and 1450 cm^{-1} showing stretching vibration of Ti-O. A peak at 873 cm^{-1} is attributed to stretching metal-oxygen bond. The multiple peaks in the frequency region 900-1650 cm^{-1} are due to the presence of Fe-O and Ag-O vibrations (absorption bands). Further, a strong and broad peak can be seen at 3435 cm^{-1} which is due to free water molecules (H_2O bands) and strong stretching (antisymmetric and symmetric) modes of the OH group. No other band appeared in the FTIR spectrum which clearly revealed the formation of $(Fe_{1/2}Ag_{1/2})TiO_3$ calcined at 750 °C. Inset of Figure 6 shows the UV-vis spectrum of FAT-nc. An absorption peak (surface plasmon resonance) was observed at 322 nm which may be due to the inter-valence charge transfer between Fe^{3+}, Ag^+ and Ti^{4+} respectively. The wavelength at the maximum exciton absorption depends upon the size of the nanoparticles which results in quantum confinements of the photo generated electron-hole carriers. Also, the plasmon bands are broadened with an absorption tail in the longer wavelengths, which may be due to the size distribution of the particles. This supports the distribution of particle sizes observed in TEM image (inset Figure 2).

Figure 7 shows the variation of real (ε') and imaginary (ε'') parts of dielectric constant with frequency at different temperatures.

It is observed that both ε'' and ε'' follows inverse dependence on frequency. The values of ε'' decrease with increase in frequency. A relatively high value of ε'' at low frequencies is normal characteristic of a dielectric material. At very low frequencies, dipoles follow the field and we have $\varepsilon' \approx \varepsilon_s$ (value of dielectric constant at quasi static fields). As the frequency increases dipoles begin to lag behind the field and ε' decreases slightly. When frequency reaches the characteristic frequency, the dielectric constant drops (relaxation process) and at very high frequencies, dipoles can no longer follow the field and $\varepsilon' \approx \varepsilon_\infty$. Also, the values of ε'' find a minimum from 200 °C onwards which shift towards higher frequency side with increasing temperature.

Figure 8 illustrates the temperature dependence of ε' and ε'' at different frequencies. It is observed that values of both ε' and ε'' first decrease and then increase with an increment in temperature during the investigated temperature range. At 334 °C ε'' finds a peak. However, no such peak was observed in case of ε', only a small step-like hump could be seen near 275 °C. The values of ε' and ε'' at room temperature are, respectively, found to be 171 and 84 at 1 kHz. Since the observation was made for only in a limited range of temperature dielectric anomaly could not be observed as similar material, e.g. $(Ag_{1/2}Bi_{1/2})TiO_3$ has very high phase transition temperature (~800 K) [4].

Figure 9 shows the variation of the real (Z') and imaginary (Z'') parts of impedance with frequency at different temperatures. It is observed that the magnitude of Z' decreases with the increase in frequency which indicates the increase in ac conductivity of the sample with increasing frequency. The values of Z'' simply increases with frequency at lower temperatures and it reaches a maximum peak (Z''_{max}) which shifts to higher frequency side with increment in temperature indicating the increasing loss in the sample. A typical peak-broadening, which is slightly asymmetrical in nature, can be observed with the rise in temperature. The broadening of peaks in frequency explicit plots of Z'' suggests that there is a spread of relaxation times *i.e.,* the existence of a temperature dependent electrical relaxation phenomenon in the material.

Figure 10 shows the complex impedance spectrum of FAT-nc at different temperatures as a Nyquist diagram. The impedance data take the shape of a semicircle in the Nyquist plots, suggesting the increasing conductivity in the sample upon heating. It can also be observed that the peak height of the plots decreases with increasing temperature and the frequency for the maximum shifts to higher values with increasing temperature. Further, it is known that for Debye-type relaxation, the centre of the semicircular plots should be located on the Z'- axis, whereas for a non-Debye type relaxation these Argand plane plots are close to semicircular arcs with end-points on the real axis and the centre lies below this axis. The complex impedance in such cases can be described as: $Z^*(\omega) = Z' + iZ'' = R[1 + (i\omega/\omega_o)^{1-\alpha}]$, where α represents the magnitude of the departure of the electrical response from an ideal condition, and this can be determined from the location of the centre of the semicircles. Also, when α approaches zero i.e. {(1-α) → 1}, the expression gives rise to classical Debye's formalism. It can be seen from the impedance plots that the data are not represented by full semicircle rather they are depressed one (i.e., centre of semicircles lies below the abscissa Z'-axis). For $\alpha > 0$, it increases with the rise in
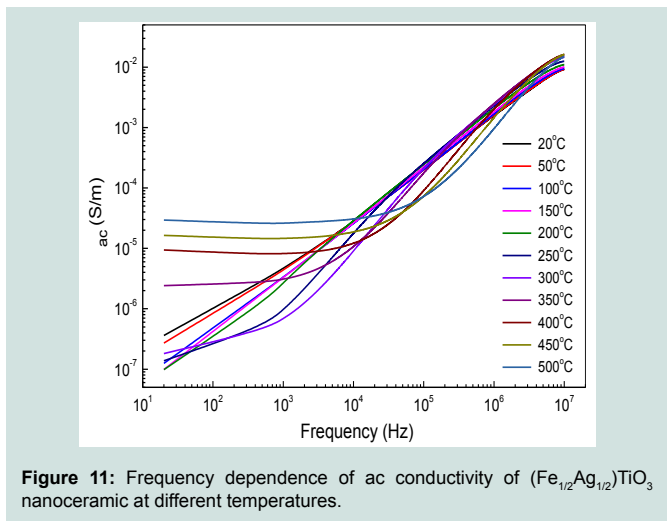
Figure 11: Frequency dependence of ac conductivity of $(Fe_{1/2}Ag_{1/2})TiO_3$ nanoceramic at different temperatures.
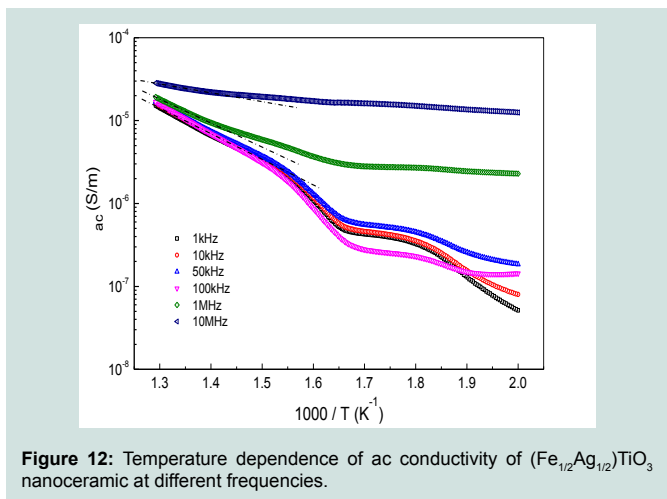

Figure 12: Temperature dependence of ac conductivity of $(Fe_{1/2}Ag_{1/2})TiO_3$ nanoceramic at different frequencies.

temperature, suggesting the dielectric relaxation to be of non-Debye type in FAT-nc. This may happen due to the presence of distributed elements in the material-electrode system.

AC conductivity data were obtained using a relation: $\sigma_{ac} = \omega\varepsilon_o\varepsilon''$. Figure 11 shows the log-log plot of ac electrical conductivity versus frequency at different temperatures for FAT-nc. The $\sigma_{ac} - f$ plots show dispersion throughout the chosen frequency range and with the increment in temperature the plots get flattened (plateau value). The switchover from the frequency-independent to the frequency-dependent regions shows the onset of the conductivity relaxation, indicating the translation from long range hopping to the short range ion-motion. Further, the electrical conductivity, in most of the materials due to localized states is expressed as Jonscher power law: $\sigma_{ac} = \sigma_o + A\omega^s$, where σ_o is the frequency-independent (electronic or dc) part of ac conductivity, s ($0 \leq s \leq 1$) is the index, ω is angular frequency of applied ac field and A is a constant, e is the electronic charge, T is the temperature, α is the polarizability of a pair of sites, and N is the number of sites per unit volume among which hopping takes place. Such variation is associated with displacement of carriers which move within the sample by discrete hops of length R between randomly distributed localized sites. The term $A\omega^s$ can

often be explained on the basis of two distinct mechanisms for carrier conduction: (i) quantum mechanical tunneling (QMT) through the barrier separating the localized sites and (ii) correlated barrier hopping (CBH) over the same barrier. In these models, the exponent s is found to have two different trends of variation with temperature and frequency. In QMT, s is predicted to be temperature independent and is expected to show a decreasing trend with ω, while for CBH, temperature dependence of s should show a decreasing trend. Furthermore, in case of perovskite-type oxide materials, presence of charge traps in the band gap of the insulator is expected. Therefore, the frequency and temperature dependence of ac conductivity supports hopping-type conduction in FAT-nc. The value of the index s was found to decrease with the rise in temperature and the value of which always remain less than 1. The model based on correlated hopping of electrons over barrier, predicts a decrease in the value of the index with the increase in temperature and so this is consistent with the experimental results. Therefore, the conduction in the system may be considered to be due to the short-range translational type hopping of charge carriers. This indicates that the conduction process is a thermally activated process.

It is observed that the hopping conduction mechanism is generally consistent with the existence of a high density of states in the materials having band gap like that of semiconductor. Due to localization of charge carriers, formation of polarons takes place and the hopping conduction may occur between the nearest neighboring sites. Figure 12 shows the variation of ac conductivity versus $10^3/T$. The activation energy for conduction was obtained using the Arrhenius relationship: $\sigma_{ac} = \sigma_o \exp(-E_a / k_B T)$, where E_a is the activation energy of conduction and T is the absolute temperature. The nature of variation shows the negative temperature coefficient of resistance (NTCR) behaviour of FAT. A linear least squares fitting of the conductivity data, at high temperatures to this equation give the value of E_a respectively to be 0.20 eV and 0.06 eV at 1 kHz and 10 MHz. It is observed that the value of activation energy decreases with the increase in frequency. It can be seen that the ac conductivity is almost in sensitive in low temperature region irrespective of the operating frequencies. Also, the onset temperature (insensitive to sensitive region) shifts to higher temperature side with the increment
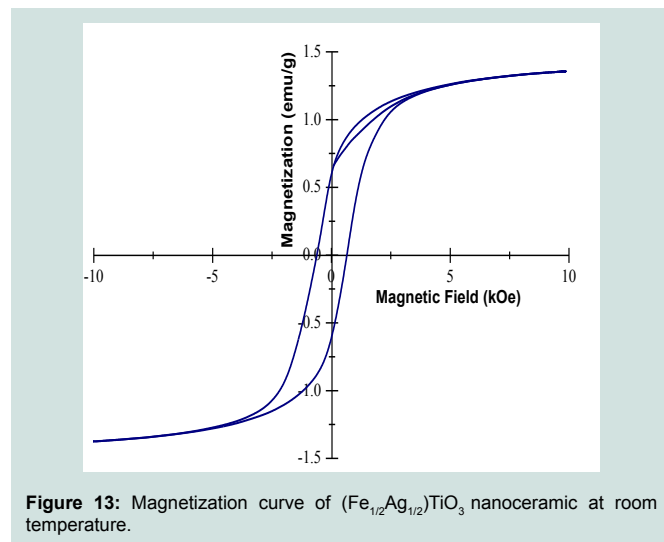

Figure 13: Magnetization curve of $(Fe_{1/2}Ag_{1/2})TiO_3$ nanoceramic at room temperature.

in frequency. The low value of E_a may be due to the carrier transport through hopping between localized states in a disordered manner. The increase in conductivity with temperature may be considered on the basis that within the bulk, the oxygen vacancies due to the loss of oxygen are usually created during sintering and the charge compensation follows the reaction: $O_o \rightarrow \frac{1}{2}O_2 \uparrow + V_o^{\bullet\bullet} + 2e^-$, which may leave behind free electrons making them n-type.

Figure 13 depicts the magnetization versus an applied field (M-H) for FAT-nc at room temperature. It is observed that M-H curve is very slim and is not completely saturated up to the applied field of 10 kOe, which indicates the size of the particles are very small (nano-sizing effect). This may be due to the fewer number of participation of Fe-Fe pairs, giving rise to low value of coercive field (H_C = 0.65 kOe) and negligible retentivity (M_R = 0.61 emu/g). Also, the saturation magnetization (M_S = 1.26 emu/g) is likewise small. This study clearly indicates that there is a possibility of magneto-electric coupling, suggesting electric ordering controlling magnetic properties at the microscopic scale. Furthermore, improved magnetic properties could be obtained compared to the previous work [12] in which the nanocrystalline powder of $(Ag_{0.5}Fe_{0.5})TiO_3$ was prepared using stearic acid gel method with aqueous $AgNO_3$.

Conclusions

In summary, the present soft-chemical method is truly a green cost-effective approach, capable of synthesizing $(Fe_{1/2}Ag_{1/2})TiO_3$ nanoceramic powder. FAT nanoceramic powder was found to have a perovskite-type monoclinic structure with the particle sizes of 16-47 nm. EDX and FTIR studies confirmed the formation of pure $(Fe_{1/2}Ag_{1/2})TiO_3$ nanoceramic. Heat of combustion, heat of dissociation of tartaric acid and combustion of organic present in the gel along with the evolution of gases during calcination created ambiance for reaction to occur more easily to form $(Fe_{1/2}Ag_{1/2})TiO_3$. UV-vis study exhibited the surface plasmon resonance at 322 nm. The dielectric relaxation was found to be of non-Debye type. The ac conductivity is found to obey the universal power law. The pair approximation type correlated barrier hopping model is found to successfully explain the mechanism of charge transport in $(Fe_{1/2}Ag_{1/2})TiO_3$ nanoceramic. Dielectric study revealed a low value of room temperature dielectric constant (= 171) and dielectric loss (= 0.49) at 1 kHz. Magnetic study indicated the possibility of magneto-electric coupling.

References

1. Rödel J, Jo W, Seifert KT, Anton EM, Granzow T, et al. (2009) Perspective on the development of lead free piezoceramics. J Am Ceram Soc 92: 1153-1177.

2. Eichel RA, Kungl H (2010) Recent developments and future perspectives of lead-free ferroelectrics. Funct Mater Lett 3: 1-4.

3. Park JH, Woodward PM, Parise JB, Reeder RJ, Lubomirsky I, et al. (1999) Synthesis, structure, and dielectric properties of $(Bi_{1/2}Ag_{1/2})TiO_3$. Chem Mater 11: 177-183.

4. Inaguma Y, Katsumata T, Wang R, Kobashi K, Itoh M, et al. (2001) Synthesis and dielectric properties of a perovskite $Bi_{1/2}Ag_{1/2}TiO_3$. Ferroelectrics 264: 127-132.

5. Wu L, Xiao D, Zhou F, Teng Y, Li Y (2011) Microstructure, ferroelectric, and piezoelectric properties of $(1-x-y)Bi_{0.5}Na_{0.5}TiO_3-xBaTiO_3-yBi_{0.5}Ag_{0.5}TiO_3$ lead-free ceramics. J Alloys Comp 509: 466-470.

6. Liao Y, Xiao D, Lin D (2008) Piezoelectric and ferroelectric properties of $Bi_{0.5}(Na_{1-x-y}K_xAg_y)_{0.5}TiO_3$ lead-free piezoelectric ceramics. Appl Phys A Mater Sci Process 90: 165-169.

7. Lu Y, Li Y, Wang D, Wang T, Yin Q (2008) Lead-free piezoelectric ceramics of $(Bi_{1/2}Na_{1/2})TiO_3-(Bi1/2K1/2)TiO3-(Bi_{1/2}Ag_{1/2})TiO_3$ system. J Electroceram 21: 309-313.

8. Raevskii IP, Reznichenko LA, Malitskaya MA (2000) Features in the dielectric properties and temperature-composition phase diagrams of $NaNbO_3-A_{0.5}Bi_{0.5}TiO_3$ (A = Li, Na, K, Ag) solid solutions. Tech Phys Lett 26: 93-95.

9. Hao J, Wang X, Chen R, Li L (2005) Synthesis of $(Bi_{0.5}Na_{0.5})TiO_3$ nanocrystalline powders by stearic acid gel method. Mater Chem Phys 90: 282-285.

10. Xu Q, Chen S, Chen W, Huang D, Zhou J, et al. (2006) Synthesis of $(Na_{0.5}Bi_{0.5})TiO_3$ and $(Na_{0.5}Bi_{0.5})_{0.92}Ba_{0.08}TiO_3$ powders by a citrate method. J Mater Sci 41: 6146-6149.

11. Kumar S, Sahay LK, Jha AK, Prasad K (2013) Synthesis and characterization of nanocrystalline $Al_{0.5}Ag_{0.5}TiO_3$ powder. Adv Nano Res 1: 211-218.

12. Kumar S, Sahay LK, Jha AK, Prasad K (2014) Synthesis of $(Ag_{0.5}Fe_{0.5})TiO_3$ nanocrystalline powder using stearic acid gel method. Adv Mater Lett 5: 67-70.

13. Kumar S, Jha AK, Prasad K (2015) Green synthesis and characterization of $(Ag_{1/2}Al_{1/2})TiO_3$ nanoceramics. Mater Sci - Poland 33: 59-72.

14. Jha AK, Kumar V, Prasad K (2011) Biosynthesis of metal and oxide nanoparticles using orange juice. J Bionanosci 5: 162-166.

15. Morrison RT, Boyd RN (1983) Advanced organic chemistry. Allyn and Bacon Inc, Boston, USA.